Preparation of solution-processed thin films of As-S-Se system from $As_{40}S_{60}$ solution modified by amorphous selenium

Jiri Jemelka[1], Karel Palka[1,*], Jiri Jancalek[2], Michal Kurka[2], Stanislav Slang[2], Miroslav Vlcek[2]

1 Department of General and Inorganic Chemistry, Faculty of Chemical Technology, University of Pardubice, Studentska 95, 53210 Pardubice, Czech Republic
2 Center of Materials and Nanotechnologies, Faculty of Chemical Technology, University of Pardubice, Studentska 95, 53210 Pardubice, Czech Republic
*karel.palka@upce.cz

Abstract

This work presents the possibility of As-S-Se chalcogenide glass thin film preparation from a solution of commercially available $As_{40}S_{60}$ glass by modification of the solution composition with elemental selenium. We studied the dissolution of elemental selenium in n-butylamine and ethylenediamine based chalcogenide glass solutions.

Samples of four compositions ranging from 0 % selenium content (pure $As_{40}S_{60}$) to 30 % selenium content ($As_{28}S_{42}Se_{30}$) were prepared by spin-coating in specular optical quality with low surface roughness (below 1 nm). Structure, refractive index, optical band gap, organic residua content, and chemical resistance were studied in dependence on the annealing temperature. The structure was studied using Raman spectroscopy, and the data suggest incorporation of selenium into the glass structure already in the solution, which resulted in an increased refractive index and reduced optical band gap of deposited thin films. Due to chalcogen over-stoichiometry, modified thin films have lower organic residua content.

Keywords

Chalcogenide glasses, Spin-coating, Thin films, Source solution modification.

Highlights

- $As_{40}S_{60}$ chalcogenide glass solution was modified by amorphous selenium.
- Spin-coated thin films of As-S-Se were deposited in specular optical quality.
- The optical properties, structure, and chemical resistance of films were studied.
- The described method allows preparation of films with tailored optical properties.

Introduction

Chalcogenide glasses are semiconducting materials with band gap values between 1-3 eV [1]. They have been widely studied for their desirable properties, such as wide transparency window in the infrared region, high refractive index, and high optical nonlinearity [1; 2]. They are also suitable for the preparation of IR optical elements such as lenses [3], diffraction gratings [4], waveguides [5], and optical switching elements [2]. The first commercially produced chalcogenide glass for bulk optical components was $As_{40}S_{60}$ in the 1950s. In the following decades, other S and Se glasses were developed, including Se-Te for the far infrared region optical components [6].

For many applications, preparing thin films of chalcogenide glasses is desirable. Traditionally these films are prepared by vacuum deposition methods, such as thermal evaporation [7], sputtering [8], or laser ablation [9]. Alternatively, thin films can be also prepared from a solution of chalcogenide glass in an amine or amine-based solvent. Thin films can be deposited from solution by various techniques, including spin-coating [10], dip-coating [11], or spray-coating [12]. Solution-based methods do not need expensive high vacuum equipment and enable composite thin film deposition from mixed solutions of chalcogenide glasses, or with doping components [13; 14; 15].

Elemental selenium is notoriously insoluble in most organic solvents, which limits its solution processability. Elemental selenium can be dissolved in an aqueous cyanide solution, amine-thiol mixtures, or hydrazine [16]. The mentioned solvents have some specific disadvantages for the

processing of selenium and selenium-based chalcogenide glasses. Notably, due to hydrolysis, aqueous solutions are not suitable for chalcogenide and chalcogenide glass dissolution. Hydrazine and thiols are highly toxic and dissolve chalcogenide glasses on a molecular level, which is not suitable for amorphous film manufacturing due to the high tendency to crystallization [16; 20]. However, selenium-based chalcogenide glass thin films have been previously reported to be successfully deposited from ethylenediamine, ethanolamine, or multi-component solutions [17; 18; 19].

In this work, we expand upon our previous work dealing with the modification of the source solution composition for thin film deposition [21]. Chalcogenide glass $As_{40}S_{60}$, commercially available as AMTIR 6 (Amorphous Materials Inc. (USA)) or IRG27 (Schott AG), was dissolved in n-butylamine and ethylenediamine and modified with amorphous selenium. N-butylamine was chosen as the most common solvent for sulfur-based chalcogenide glasses and ethylenediamine as the most common solvent for selenium-based chalcogenide glasses. Modification of the source solution allows easy and predictable tailoring of the optical properties (refractive index and optical band gap).

We studied optical properties (refractive index at wavelength 1550nm n_{1550} and optical band gap E_g^{opt}), thickness (d), surface roughness, structure, organic residua content, and chemical resistance of the deposited chalcogenide thin films.

Experimental

The bulk chalcogenide glass of $As_{40}S_{60}$ composition was synthesized using the standard melt-quench method. Stoichiometric amounts of pure 5N elements were weighted into a quartz ampoule and sealed under vacuum (10^{-3} Pa). The synthesis was conducted in a rocking tube furnace at 850°C for 32 hours. After synthesis, the ampoule was quenched in cold water.

Amorphous selenium was prepared from pure 5N selenium using the melt-quench method. Selenium was introduced into the quartz ampoule and sealed under a vacuum (10^{-3} Pa). The selenium was heated in a rocking tube furnace to 500°C for 8 hours and afterward quenched in cold water.

The bulk glass $As_{40}S_{60}$ was pulverized in an agate bowl and afterward dissolved in n-butylamine (BA) and ethylenediamine (EDA) under a nitrogen atmosphere in a glovebox. The concentrations of $As_{40}S_{60}$ solutions were adjusted, so the concentration of the resulting glass solution (after selenium doping) of the targeted composition was 0.1g/ml of BA, and 0.15g/ml of EDA. Glass dissolution was performed under intensive stirring with a magnetic stirrer. After the glass dissolved, the calculated amount of amorphous selenium was dissolved in $As_{40}S_{60}$ solution while agitated by vortex mixer Classic (Velp). Solutions of 4 different compositions were prepared: $As_{40}S_{60}$ (hereafter referred to as 0 % Se), $As_{36}S_{54}Se_{10}$ (hereafter referred to as 10 % Se), $As_{32}S_{48}Se_{20}$ (hereafter referred to as 20 % Se), $As_{28}S_{42}Se_{30}$ (hereafter referred to as 30 % Se).

Chalcogenide glass thin films were deposited by the spin-coating method. The chalcogenide glass solutions were pipetted onto rotating soda-lime substrates and spin-coated (spin-coater Laurell WS-650Mz-23NPPB) in a nitrogen atmosphere for 60 s at a spin-rate of 5000 RPM for the BA-based solutions and 2000 RPM for EDA-based. Deposited thin films were annealed at 60 °C on a hot plate for 20 min (hereafter referred to as "as-prepared" thin films). The as-prepared thin films were subsequently annealed at temperatures 90, 120, 150, and 180 °C for 1 hour on a hot plate in a nitrogen-filled glovebox. The temperature range was chosen based on a preliminary experiment, with respect to the glass transition temperature of the used glasses (T_g = 184°C for $As_{40}S_{60}$, T_g = 150°C for $As_{33}S_{67}$, T_g = 125°C for $As_{28.6}S_{71.4}$, T_g = 150°C for $As_{40}Se_{60}$, T_g = 135°C for $As_{33}Se_{67}$, T_g = 112°C for $As_{28.6}Se_{71.4}$) [22; 23] in order to obtain thin films with specular optical quality and low organic residua content.

Transmission spectra were measured using UV-VIS-NIR spectrometer UV3600 (Shimadzu) for the spectral range of 190 – 2000 nm. Transmission spectra of all studied thin films are provided in supplementary materials in Figs. 1S and 2S. The thickness and refractive index of the prepared thin films were determined from the transmission spectra using the fitting procedure described in [24] based on a combination of Swanepoel's model of thin film on a finite substrate [25] and the Wemple-DiDomenico's equation [26]. The optical band gap was determined using Tauc's method for semiconductors [27]. Transmission spectra were measured on three samples for each annealing temperature and thin film composition. The presented values of thickness and optical parameters

represent the average values of experimental results, and standard deviations from these average values are provided as the error bars.

The structure of both thin films and solutions was studied by Raman spectroscopy. Measurements were performed on MultiRAM (Bruker) FT-Raman spectrometer using 1064 nm Nd:YAG excitation laser (resolution 2 cm^{-1}, average of 64 scans for thin films and 200 scans for chalcogenide glass solutions). The resulting spectra of thin films were normalized by the intensity of the most intensive band. Solution spectra were normalized by the intensity of the most intensive band of the pure solvent (400 cm^{-1} for BA and 475 cm^{-1} for EDA).

A LYRA 3 scanning electron microscope (Tescan) equipped with an EDS analyzer Aztec X-Max 20 (Oxford Instrument) was used to study elemental composition. Samples were measured on five 400 x 400 µm areas at accelerating voltage of 5 kV. The presented data show the average of five values, and the standard deviation is given as an error bar.

The thin film surface roughness and topography were studied using atomic force microscopy (AFM) in semi-contact mode using NTEGRA (NT-MDT) microscope equipped with HA_HR tips (ScanSens). Three areas of 5 x 5 µm were measured for each annealing temperature and thin film composition. AFM scans of all studied thin films are provided in supplementary materials in Figs. 3S and 4S. The presented values of RMS (calculated according to ISO 4287/1 norm) are the average values of three scans with error bars representing standard deviations.

The chemical resistance of the thin films was studied by etching thin films in a solution of 5 vol.% n-butylamine in dimethyl sulfoxide at 25°C. The etching rates were evaluated as described in [28].

Results and Discussion

Selenium is insoluble in pure BA and slightly soluble in EDA [16], therefore it is not possible to prepare a selenium solution using these solvents alone. However, we have found out that selenium readily dissolves in As-S chalcogenide glass solutions in both BA and EDA. During preliminary experiments, we observed an increased dissolution rate of selenium in stoichiometric $As_{40}S_{60}$ chalcogenide glass solution compared to sulfur-rich chalcogenide glass solutions ($As_{30}S_{70}$, $As_{33}S_{67}$). We assume that As-rich clusters which are more abundant in stoichiometric glass are responsible for the enhanced solubility as they can provide reactive As-As homopolar bonds.

The solubility of elemental selenium strongly depends on its crystallographic modification [16]. Although crystalline selenium is also soluble in both BA-based and EDA-based 10% Se chalcogenide glass solution, amorphous selenium dissolves significantly faster (especially in BA-based solution), therefore it is more suitable for compositional modification. Amorphous selenium dissolved in 5 to 30 minutes depending on concentration. Figure 1 shows the photos of selenium-modified chalcogenide glass solutions and their gradual color change from yellow to dark red with increasing selenium content.

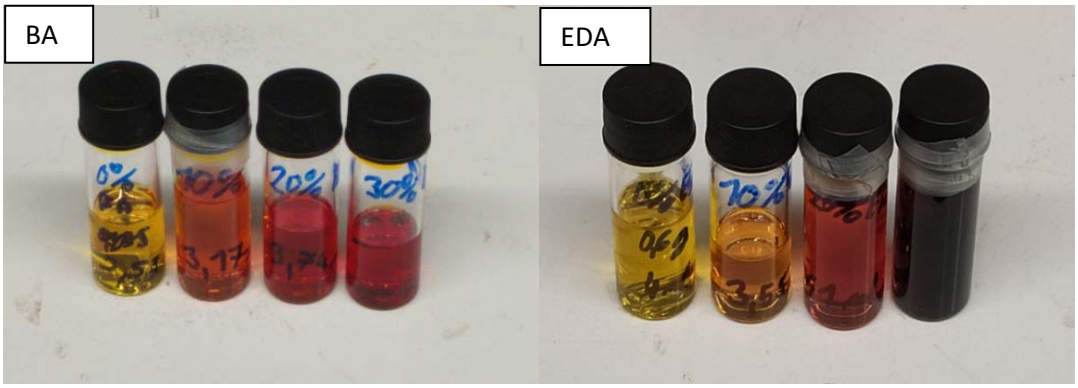

Figure 1 – Photos of BA-based (left) and EDA-based (right) chalcogenide glass solutions with increasing Se content (from left to right 0 % Se, 10 % Se, 20 % Se, 30 % Se).

The optical properties of the thin films prepared from BA and EDA-based solutions were evaluated using UV-VIS-NIR transmission spectra. The experiments confirmed that the optical quality of EDA-based thin films is superior to that of BA-based thin films. While the EDA-based thin films have specular optical quality (interference maxima reaches the transmission of the substrate), BA-based samples containing selenium show visible optical defects (such as lowered optical transmission or opacity of thin films), especially at lower annealing temperatures. For this reason, the optical parameters of the BA-based thin film could not be reliably determined. Only the thickness of BA-based thin films is presented, but the accuracy of its determination may be affected by the poor quality of the samples. Examples of UV-VIS-NIR transmission spectra for BA-based thin film and EDA-based thin films annealed at 120°C are shown in Figure 2, and spectra of all compositions and annealing temperatures are presented in Figure 1S and 2S in supplementary materials.

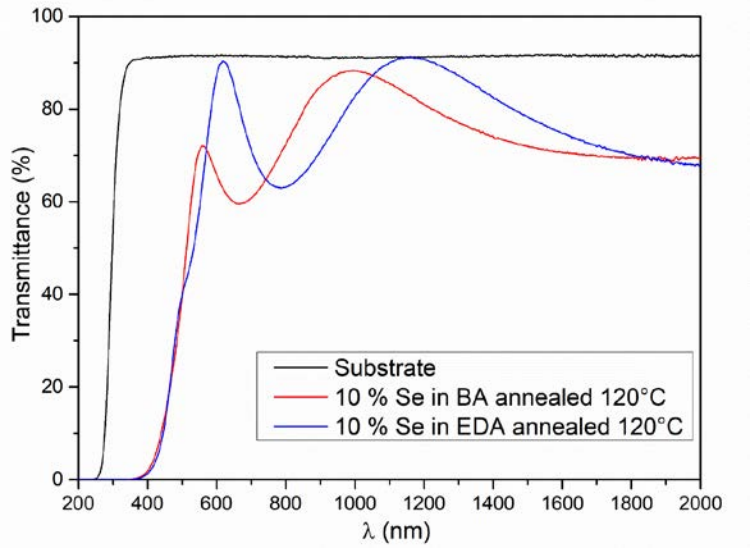

Figure 2 – Example UV-VIS-NIR transmission spectra of thin films deposited from modified solutions (10% Se in BA and EDA, T=120°C).

The EDA-based samples possessed specular optical quality in the whole studied temperature range. The values of film thickness *d*, the refractive index at 1550 nm $n_{1550,}$ and optical band gap E_g^{opt} were evaluated according to the procedure described in [24] and results are presented in Table 1. The dependence of thin film thickness and refractive index on both selenium content and annealing temperature are shown in Figure 3.

The thickness of the as-prepared EDA-based thin films is almost similar for 0 % Se, 10% Se, and 20 % Se but drops significantly for 30 % Se samples. We assume that this may be due to changes in EDA-based glass solution, which are visible on Raman spectra and will be discussed later. The data also show a decrease in film thickness with increasing selenium content, despite the same source solution concentration in the annealed samples.

We observed a decrease in the thickness and an increase in the refractive index of thin films with increasing annealing temperature due to the release of organic solvent molecules and decomposition of alkyl ammonium arsenic sulfide salts [29]. Contrary, the optical band gap doesn't show any significant dependence on the annealing temperature. Additionally, we observed a significant increase in the refractive index and a decrease in the band gap with increasing selenium content. This observation is in line with the compositional dependencies described by other authors [30; 31; 32].

The BA-based samples exhibit high variance in the thickness of as-prepared samples, while the thickness of annealed samples regularly decreases with rising Se content. The probable cause of this behavior will be further discussed later.

Table 1 - Thickness, refractive index at wavelength 1550 nm, and optical band gap of thin films in dependence on annealing temperature and composition.

	0 % Se in BA	10 % Se in BA	20 % Se in BA	30 % Se in BA
T [°C]	d [nm]	d [nm]	d [nm]	d [nm]
as-prepared	235.6 ± 10.1	290.8 ± 3.6	234.2 ± 5	207.4 ± 7.6
90	217.8 ± 9.5	260.9 ± 5.2	204.5 ± 5.7	156.2 ± 1.5
120	204.1 ± 6.9	208.4 ± 2.2	171.4 ± 18.1	148.8 ± 0.9
150	199.5 ± 10.4	179.2 ± 8.4	156.3 ± 4.7	133.1 ± 3.5
180	171.1 ± 14.8	166.1 ± 13.7	133.8 ± 1.2	121.1 ± 3.6

	0 % Se in EDA	10 % Se in EDA	20 % Se in EDA	30 % Se in EDA
T [°C]	d [nm]	d [nm]	d [nm]	d [nm]
as-prepared	284.9 ± 3.4	286.9 ± 5.5	283.5 ± 5.3	245.8 ± 1.7
90	266.9 ± 4.0	258.5 ± 3.2	250.8 ± 1.8	221.9 ± 2.9
120	253.0 ± 1.9	243.6 ± 1.1	234.6 ± 1.0	205.2 ± 1.8
150	238.6 ± 2.6	233.0 ± 0.8	210.2 ± 0.6	181.4 ± 1.1
180	209.6 ± 0.9	209.0 ± 1.0	187.7 ± 1.7	163.6 ± 0.9

	0 % Se in EDA	10 % Se in EDA	20 % Se in EDA	30 % Se in EDA
T [°C]	n_{1550}	n_{1550}	n_{1550}	n_{1550}
as-prepared	2.23 ± 0.00	2.22 ± 0.02	2.24 ± 0.01	2.26 ± 0.01
90	2.26 ± 0.02	2.29 ± 0.02	2.32 ± 0.02	2.32 ± 0.01
120	2.31 ± 0.02	2.35 ± 0.00	2.37 ± 0.01	2.38 ± 0.01
150	2.33 ± 0.02	2.36 ± 0.01	2.40 ± 0.01	2.44 ± 0.01
180	2.34 ± 0.00	2.43 ± 0.01	2.46 ± 0.01	2.50 ± 0.01

	0 % Se in EDA	10 % Se in EDA	20 % Se in EDA	30 % Se in EDA
T [°C]	E_g^{opt} [eV]	E_g^{opt} [eV]	E_g^{opt} [eV]	E_g^{opt} [eV]
as-prepared	2.30 ± 0.01	2.17 ± 0.01	2.07 ± 0.00	1.98 ± 0.02
90	2.26 ± 0.00	2.13 ± 0.00	2.06 ± 0.00	1.99 ± 0.00
120	2.25 ± 0.00	2.13 ± 0.01	2.06 ± 0.01	1.97 ± 0.00
150	2.23 ± 0.00	2.13 ± 0.01	2.08 ± 0.00	1.96 ± 0.02
180	2.25 ± 0.00	2.18 ± 0.00	2.07 ± 0.01	1.91 ± 0.02

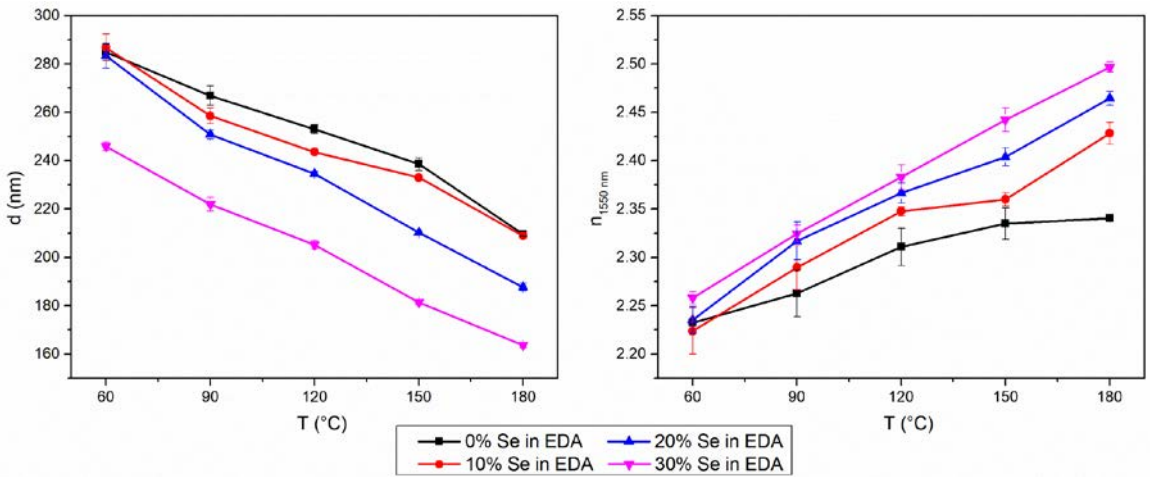

Figure 3 – Dependence of thin film thickness (left) and refractive index at wavelength 1550 nm (right) on annealing temperature and composition for EDA-based thin films.

The selenium-modified EDA-based thin films exhibit higher surface roughness of as-prepared thin films than annealed films. The roughness of annealed thin films sharply decreases even at the lowest annealing temperature (Table 2) and doesn't affect the optical properties of the thin films. All annealed samples show low surface roughness (below 1 nm) and no significant structural defects detectable by AFM (Figure 3S).

The BA-based selenium-modified thin films exhibit high surface roughness and porosity that at first increases up to a certain temperature (90°C or 120°C depending on selenium content) and later significantly decreases after annealing at higher temperatures (Table 3 a Figure 4S). A decrease in surface roughness at higher annealing temperatures may be induced by surface diffusion and viscous flow [33]. Observed high surface roughness might be a probable cause of decreased optical quality of BA-based selenium-modified thin films. AFM scans in Figure 3S and 4S further support our claim, that BA-based thin films exhibit high porosity.

Table 2 – Surface roughness of EDA-based thin films of all studied compositions at all annealing temperatures.

T [°C]	0 % Se in EDA	10 % Se in EDA	20 % Se in EDA	30 % Se in EDA
as-prepared	0.36 ± 0.03	1.52 ± 0.15	2.5 ± 0.29	2.13 ± 0.37
90	0.32 ± 0.11	0.48 ± 0.07	0.31 ± 0.01	0.47 ± 0.04
120	0.44 ± 0.14	0.23 ± 0.04	0.21 ± 0.01	0.27 ± 0.05
150	0.36 ± 0.12	0.26 ± 0.04	0.25 ± 0.01	0.26 ± 0.04
180	0.3 ± 0.02	0.35 ± 0.02	0.25 ± 0.03	0.32 ± 0.04

Table 3 – Surface roughness of BA-based thin films of all studied compositions at all annealing temperatures.

T [°C]	0 % Se in BA	10 % Se in BA	20 % Se in BA	30 % Se in BA
as-prepared	0.5 ± 0.04	4.52 ± 0.34	5.86 ± 1.49	6.27 ± 0.55
90	0.42 ± 0.02	5.07 ± 0.41	13.02 ± 0.82	6.49 ± 1.28
120	0.3 ± 0.01	6.86 ± 0.33	5.02 ± 0.45	1.73 ± 0.3
150	0.32 ± 0.06	0.43 ± 0.02	0.38 ± 0.12	0.48 ± 0.21
180	0.3 ± 0.01	0.42 ± 0.02	0.66 ± 0.13	0.32 ± 0.04

The compositions of both BA and EDA-based thin films were analyzed by EDS. The compositions of as-prepared thin films matched the calculated values with only slightly decreased arsenic content (by approximately 2 %) as shown in figure 4. This can be explained by the partial oxidation of arsenic during the transport under ambient conditions to EDS analysis and subsequent evaporation of arsenic oxide in a vacuum chamber of the electron microscope. This phenomenon has been previously described in our earlier work [34].

We observed a significant decrease in sulfur content at higher annealing temperatures in selenium-modified samples. This can be explained by the partial evaporation of over-stoichiometric sulfur. This is supported by the fact that the sulfur content decrease is strongly dependent on the glass stoichiometry. Sulfur depletion was not observed in the $As_{40}S_{60}$ thin film due to its stoichiometry (no excess sulfur) and regularly increased with higher sulfur and selenium over-stoichiometry. The absolute value of selenium content remains unchanged despite the sulfur depletion, which indicates that selenium is also partially vaporized. Samples containing 30 % Se differ significantly between BA and EDA-based samples. We think that the high porosity of the as-prepared thin films and low T_g could facilitate sulfur evaporation.

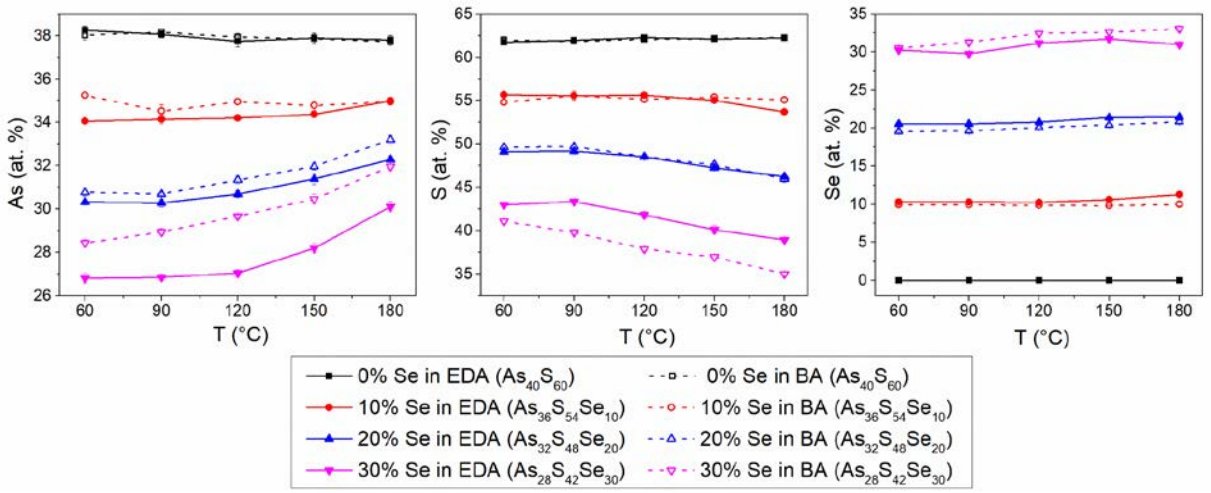

Figure 4 – Dependencies of As, S, and Se content on annealing temperature for studied glass compositions.

The nitrogen content was studied to determine the organic residua content (from solvent) in the deposited thin films. As shown in Figure 5, EDA-based thin films show a strong correlation between organic residua content and their chalcogen over-stoichiometry. With increasing selenium content, the organic residua content in annealed films decreases. This is partially due to increased Se content, and partially due to a significant change in glass stoichiometry. Both phenomena were previously observed and explained in our previous works [34; 17]. Although a different solvent was used, the overall results are in good agreement.

BA-based thin films show no strong compositional dependence on organic residua content. The higher layer thickness of 10 % Se samples, despite their lower organic residua content, probably indicates high film porosity. This theory is further supported by AFM scans (Figure 4S) and by the increased surface roughness. High porosity can explain the lower residua content of these films because evaporating solvent escapes easily through a porous layer.

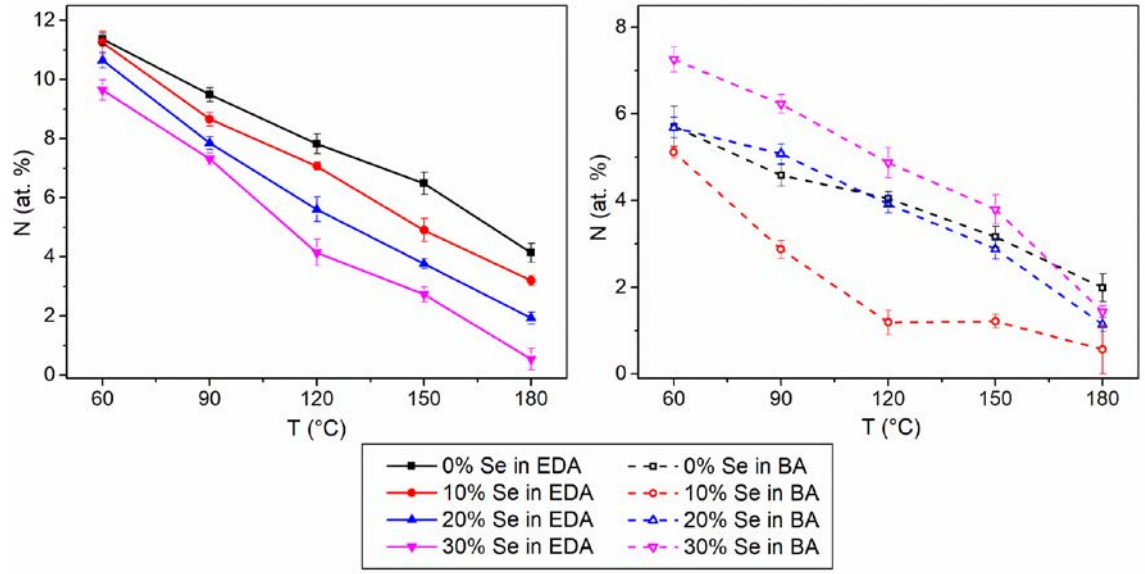

Figure 5 – Nitrogen content in thin films in dependence on annealing temperature and thin film composition.

Raman spectra of both pure solvents (BA and EDA) and solutions of all glass compositions were measured to investigate the structural units present in prepared solutions. The spectra were normalized by the most intensive peak in the 200-500 cm^{-1} region for pure solvent (400 cm^{-1} for BA and 475 cm^{-1} for EDA) and are presented in Figure 6.

The most significant change in Raman spectra in dependence on the solution composition for both BA and EDA-based solutions was observed for the 267 cm^{-1} band, which corresponds to Se_8 ring vibration [35; 36]. This band is not present in the $As_{40}S_{60}$ glass solution and then grows proportionally with increasing selenium content. A weaker band at 244 cm^{-1} appears and grows with increasing selenium content. We assume this band could be attributed to Se-chains [35; 36]. With increasing selenium content, the bands at 328cm^{-1} and 376 cm^{-1}, probably corresponding to As_4S_4 vibrations [37], gradually weaken due to the lowering concentration of As_4S_4 structural units in a chalcogenide-rich glass. The weak band at 406 cm^{-1}, probably corresponding to polysulfides and sulfur radicals [37; 38], rises with increasing selenium content due to increased free sulfur content and is observable only in the Raman spectra of the EDA-based solution (the intensive BA band at 400 cm^{-1} overlaps with its position).

The bands at 352, 484, and 500 cm^{-1} in BA-based solutions correspond to the bands of pure BA. The band at 438 cm^{-1} probably belongs to S-S stretching bond vibration and should rise with increasing free sulfur content. However the exact nature of this band or overlapping bands is not determined yet [35; 37]. According to Guiton [37], the bands at 197 cm^{-1} and 215 cm^{-1} correspond to As_4S_4 structural unit vibration and are present only in spectra of unmodified samples. In the EDA-based solutions, we observed a weak band at around 300 cm^{-1} which shifted to higher wavenumbers with increasing selenium content. We think this band can be attributed to some As-S-Se dissolution products whose composition changes with increasing selenium content. This could explain the color change and the smaller thickness of the as-prepared 30 % Se EDA-based samples, as it suggests a significant change in the dissolution product structure.

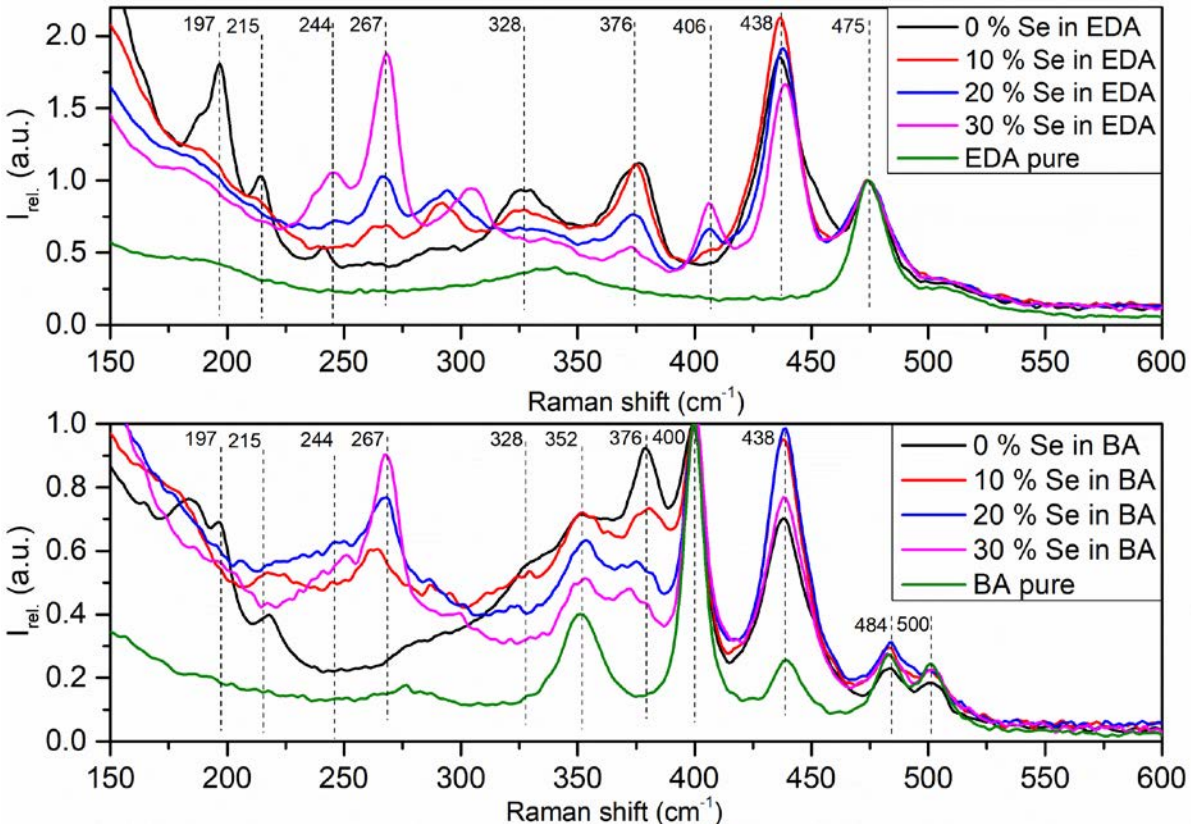

Figure 6 – Raman spectra of BA and EDA-based chalcogenide glass solutions modified by selenium.

Raman spectra of BA and EDA-based thin films of all compositions were measured for both as-prepared and annealed thin films (Raman spectra of 180°C annealed thin films are not shown due to the present highly intensive luminescence). The spectra of both BA and EDA-based thin films exhibit the same trends and will be discussed together. Raman spectra of thin films are presented in Figure 7.

The most significant band for the 0% Se sample ($As_{40}S_{60}$) is situated at 342 cm^{-1} and corresponds to the vibration of $AsS_{3/2}$ pyramidal units [21; 39; 40]. The intensive band at 373 cm^{-1} can be assigned to the vibration of As_4S_4 cluster units [21; 39; 40]. The band at 312 cm correspond to different vibration of the $AsS_{3/2}$ pyramidal units [21; 39; 40]. The weak band at 420 cm^{-1} corresponds to alkyl ammonium arsenic sulfide salts (AAAS) [29].

The selenium-modified samples exhibit two new bands in the Raman spectra. An intensive band at 259 cm^{-1} corresponds to the vibration of Se_8 rings [35; 39], and a weaker band at 232 cm^{-1} can correspond to either Se-chains [35; 39] or $AsSSe_2$ mixed pyramidal units [24; 39].

The most significant trend in Raman spectra is the appearance and subsequent growth of band corresponding Se_8 rings with increasing selenium content. The weaker band corresponding to Se-chains or mixed $AsSSe_2$ pyramids grows with increasing selenium content and with increasing annealing temperature, which suggests the incorporation of previously separated Se_8 rings into the glass structure. Another significant change with increasing annealing temperature is decreased intensity of the band corresponding to As_4S_4 and an increase in the intensity of bands corresponding to $AsS_{3/2}$. This indicates the reaction of As_4S_4 with excess sulfur and polymerization of the glass structure. The decomposition of AAAS salts can also be observed at elevated annealing temperatures.

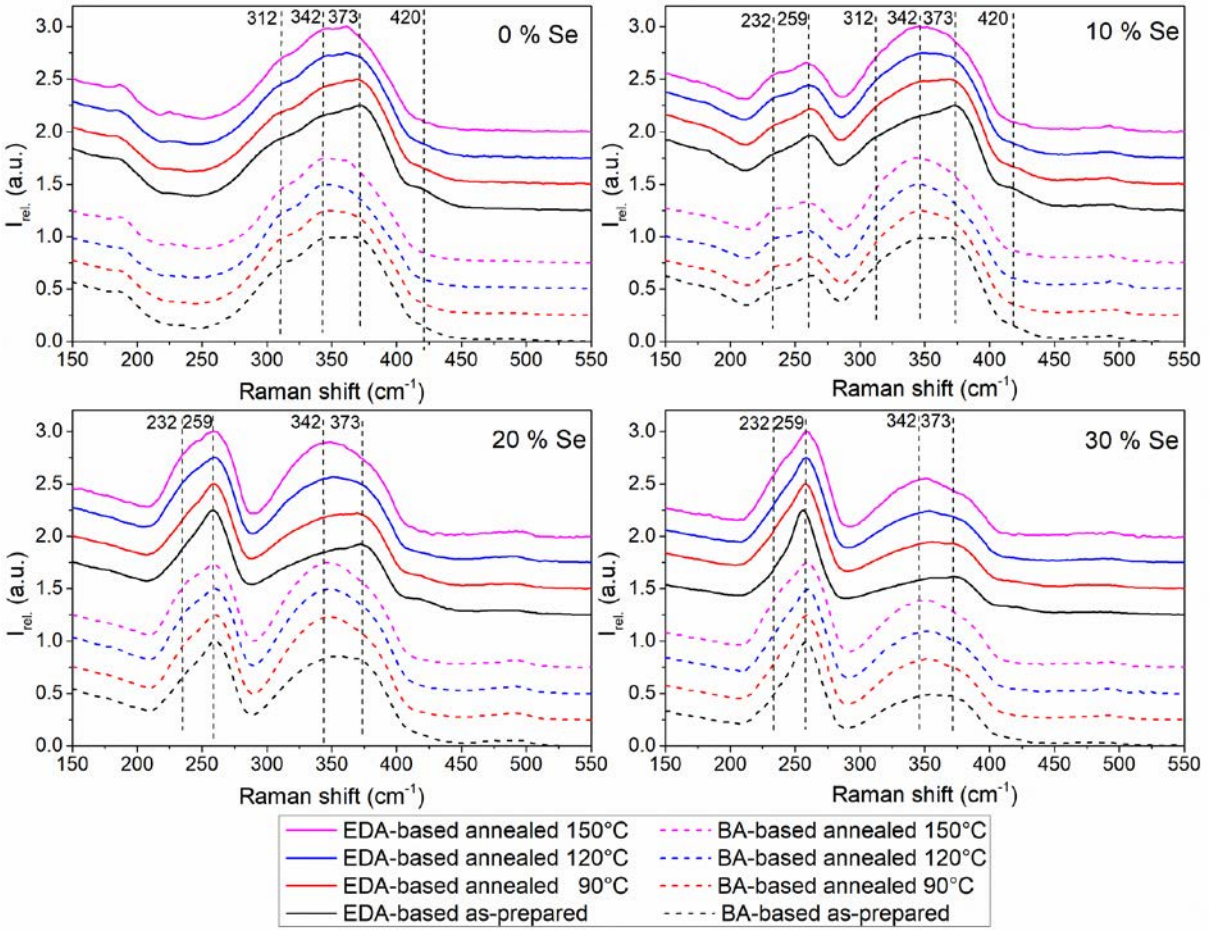

Figure 7 – Raman spectra of thin films in dependence on annealing temperature and thin film composition.

The chemical resistance of the thin films was studied by measuring the etching kinetics in 5 vol.% BA in dimethyl sulfoxide solution at 25°C. For both BA-based and EDA-based thin films, a significant dependence of etching rate on both composition and annealing temperature was observed. With increasing annealing temperature, the etching rate decreases due to organic residua release and polymerization of the glass structure, as discussed in the previous chapter. Also, with increasing selenium content, the etching rate increases significantly for both BA and EDA-based thin films. Chalcogenide glasses of the As-Se system are usually chemically more resistant than As-S glasses of the same element ratio [17; 41]. The Raman spectra suggest at least partial incorporation of selenium into the glass structure, which should increase the chemical resistance. However, this effect is counteracted by the change in the ratio of arsenic to chalcogen. Glasses with a lower arsenic-to-chalcogen ratio are generally less chemically resistant, because of their less polymerized structure [21] (lower content of trivalent arsenic). This effect dominates in this case, as demonstrated by Figure 8.

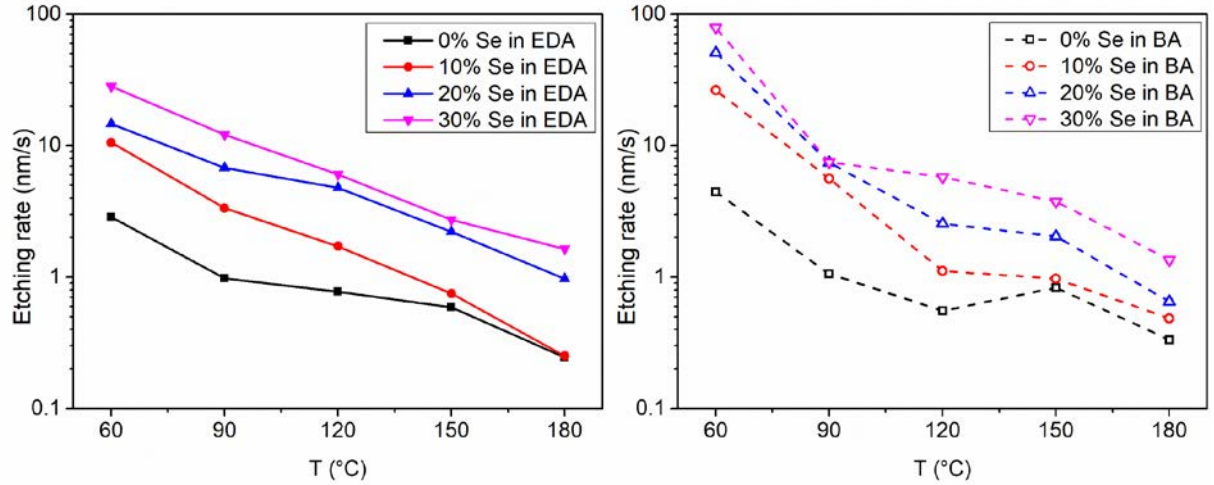

Figure 8 – Chemical resistance of thin film in dependence on annealing temperature and thin film composition.

Conclusion

Thin films of the As-S-Se glass system were prepared from BA and EDA-based solutions of $As_{40}S_{60}$ directly modified by amorphous selenium. The EDA-based thin films were deposited in specular optical quality and low surface roughness, but BA-based thin films exhibited lower optical quality and observable porosity. The structure and composition of the thin films were studied, and the results suggest the incorporation of selenium into the glass structure already in the solution phase. During annealing, the release of residual solvent and polymerization of the glass structure was observed by EDX and Raman spectroscopy. With increasing selenium content, an increase in refractive index and a decrease in optical band gap was observed, as well as reduced chemical resistance of the selenium-rich thin films.

This method allows easy and precise tailoring of glass composition and thus optical properties. The disadvantage of this method is the limited range of solutions that can be achieved using this method. This method allows more cost-effective and simpler manufacturing of chalcogenide glass optical elements requiring various optical properties.

CRediT author statement

Jiri Jemelka: Conceptualization, Investigation, Writing - Original Draft, Formal analysis Visualization.
Karel Palka: Conceptualization, Validation, Supervision, Writing - Review & Editing, Resources
Jiri Jancalek: Investigation, Methodology, Formal analysis, Writing - Review & Editing, Validation.
Michal Kurka: Investigation, Methodology, Formal analysis, Writing - Review & Editing, Validation.
Stanislav Slang: Investigation, Writing - Review & Editing, Formal analysis, Validation, Methodology.
Miroslav Vlcek: Supervision, Funding acquisition, Writing - Review& Editing, Validation.

Fundings

Authors appreciate the financial support from grant LM2018103 from the Ministry of Education, Youth and Sports of the Czech Republic and European Regional Development Fund-Project "High-sensitive and low density materials based on polymeric nanocomposites – NANOMAT (CZ.02.1.01/0.0/0.0/17_048/0007376).

Disclosures

The authors declare no conflicts of interest.

Reference

1. K. Tanaka, K. Shimakawa. Amorphous chalcogenide semiconductors and related materials. New York: Springer, 2021. ISBN 978-1-4419-9509-4.
2. A. Zakery, S.R. Elliott. Optical properties and applications of chalcogenide glasses: a review. J. Non-Cryst. Solids. 1-3, 2003, Vol. 330, 1-12.
3. T. Zhou, X. Liu, Z. Zhu, Z. Liang, X. Wang. A Review of the Precision Glass Molding of Chalcogenide Glass (ChG) for Infrared Optics. Micromachines. 2018, Vol. 9, 7 (337).
4. N. Ostrovsky, D. Yehuda, S. Tzadka, E. Kassis, S. Joseph, M. Schvartzman. Direct Imprint of Optical Functionalities on Free-Form Chalcogenide Glasses. Adv. Opt. Mater. 2019, Vol. 7, 19.
5. P. Jean, A. Douaud, S. LaRochelle, Y. Messaddeq, W. Shi. Silicon subwavelength grating waveguides with high-index chalcogenide glass cladding. Opt. Express. 2021, Vol. 29, 13, 20851-20862.
6. N. Mehta. Applications of chalcogenide glasses in electronics and optoelectronics: A review. J. Sci. Ind. Res. 2006, Vol. 65, 10, 777-786.
7. J. Orava, T. Kohoutek, T. Wagner. Deposition techniques for chalcogenide thin films. Chalcogenide Glasses. s.l. : Woodhead Publishing, 2014, 265-309.
8. T. Halenkovic, J. Gutwirth, P. Nemec, E. Baudet, M. Specht, Y. Gueguen, J.-C. Sangleboeuf, V. Nazabal. Amorphous Ge-Sb-Se thin films fabricated by co-sputtering Properties and photosensitivity. J. Am. Ceram. Soc. 2018, Vol. 101, 7, 2877-2887.
9. G. Bulai, O. Pompilian, S. Gurlui, P. Nemec, V. Nazabal, N. Cimpoesu, B. Chazallon, C. Focsa. Ge-Sb-Te Chalcogenide Thin Films Deposited by Nanosecond, Picosecond, and Femtosecond Laser Ablation. Nanomaterials. 2019, Vol. 9, 5.
10. S. Slang, P. Janicek, K. Palka, and M. Vlcek. Structure and properties of spin-coated Ge25S75 chalcogenide thin films. Opt. Mater. Express. 2016, Vol. 6, 6, 1973-1985.
11. K. Mokurala, S. Mallick, P. Bhargava, S. Siol, T.R. Klein, M.F.A.M. van Hest. Influence of dipping cycles on physical, optical, and electrical properties of Cu2NiSnS4: Direct solution dip coating for photovoltaic applications. J. Alloys Compd. 2017, Vol. 725, 510-518.
12. P. Arnou, M.F.A.M. van Hest, C. S. Cooper, A.V. Malkov, J.M. Walls, and J.W. Bowers. Hydrazine-Free Solution-Deposited CuIn(S,Se)2 Solar Cells by Spray Deposition of Metal Chalcogenides. ACS Appl. Mater. Interfaces. 2016, Vol. 8, 13, 11893-11897.
13. C. R. Mendon, J.M.P. Almeida, E.C. Barbano, C.B. Arnold, L. Misoguti. Nonlinear optical waveguides in As2S3-Ag2S chalcogenide glass thin films. Opt. Mater. Express. 2017, Vol. 7, 1, 93-99.
14. S. Novak, L. Scarpantonio, J. Novak, M. Dai Pre, A. Martucci, J.D. Musgraves, N.D. McClenaghan, K. Richardson. Incorporation of luminescent CdSe/ZnS core-shell quantum dots and PbS quantum dots into solution-derived chalcogenide glass films. Opt. Mater. Express. 2013, Vol. 3, 6, 729-738.
15. M.V. Kovalenko, R.D. Schaller, D. Jarzab, M.A. Loi, D.V. Talapin. Inorganically Functionalized PbS–CdS Colloidal Nanocrystals: Integration into Amorphous Chalcogenide Glass and Luminescent Properties. J. Am. Chem. Soc. 2012, Vol. 134, 5, 2457–2460.
16. D.H. Webber, J.J. Buckley, P.D. Antuneza, R.L. Brutchey. Facile dissolution of selenium and tellurium in a thiol–amine solvent mixture under ambient conditions. Chem. Sci. 2014, Vol. 5, 6, 2498-2502.
17. S. Slang, K. Palka, P. Janicek M. Grinco, M. Vlcek. Solution processed As30Se70 chalcogenide glass thin films with specular optical quality: multi-component solvent approach. Opt. Mater. Express. 2018, Vol. 8, 4, 948-959.

18. Y. Zou, H. Lin, O. Ogbuu, L. Li, S. Danto, S. Novak, J. Novak, J.D. Musgraves, K. Richardson, J. Hu. Effect of annealing conditions on the physio-chemical properties of spin-coated As2Se3 chalcogenide glass films. Opt. Mater. Express. 2012, Vol. 2, 12, 1723-1732.
19. Prince, R. Singh, M. Zulfequar, A. Kumar, P. K. Dwivedi. Electrical and optical properties of solution phase deposited As2S3 and As2Se3 chalcogenide thin films: A comparative study with thermally deposited films. J. Non-Cryst. Solids. 2017, Vol. 476, 46-51.
20. C.L. McCarthy, R.L. Brutchey. Solution processing of chalcogenide materials using thiol–amine "alkahest" solvent systems. Chem. Commun. 2017, Sv. 53, 4888-4902.
21. K. Palka, S. Slang, J. Jancalek and M. Vlcek. Modification of solution processed thin chalcogenide films composition by source solution doping. J. Non-Cryst. Solids. 2019, Vol. 517, 76-82.
22. Z.U. Borisova. Glassy Semiconductors. New York: Springer New York, 1981. 505. ISBN 978-1-4757-0853-0.
23. M. Frumar, T.Kohoutek, T.Wagner, J.Orava, M.Krbal, A.Fejfar, T.Mates, S.O. Kasap. Surface morphology of spin-coated As–S–Se chalcogenide thin films. J. Non-Cryst. Solids. 2007, Vol. 353, 13, 1437-1440.
24. K. Palka, S. Slang, J. Buzek, M. Vlcek. Selective etching of spin-coated and thermally evaporated As30S45Se25 thin films. J. Non-Cryst. Solids. 2016, Vol. 447, 104-109.
25. R. Swanepoel. Determination of the thickness and optical constants of amorphous silicon. J. Phys. E. Sci. Instrum. 1983, Vol. 16, 12, 1214.
26. S.H. Wemple, M. DiDomenico. Behavior of the Electronic Dielectric Constant in Covalent and Ionic Materials. Phys. Rev. B. 1973, Vol. 3, 4, 1338.
27. J. Tauc. Absorption edge and internal electric fields in amorphous semiconductors. Mater. Res. Bull. 1970, Vol. 5, 8, 721-729.
28. L. Loghina, K. Palka, J. Buzek, S. Slang, M. Vlcek. Selective wet etching of amorphous As2Se3 thin films. J. Non-Cryst. Solids. 2015, Vol. 430, 21-24.
29. S. Slang, K. Palka, L. Loghina, A. Kovalskiy, H. Jain, M. Vlcek. Mechanism of the dissolution of As–S chalcogenide glass in n-butylamine and its influence on the structure of spin coated layers. J. Non-Cryst. Solids. 2015, Vol. 426, 125-131.
30. J. Tasseva, V. Lozanova, R. Todorov, K. Petkov. Optical characterization of Ag/As-S-Se thin films. J. Optoelectron. Adv. Mater. 2007, Vol. 9, 10, 3119 - 3124.
31. T. Cardinal, K.A. Richardson, H. Shim, A. Schulte, R. Beatty, K. Le Foulgoc, C. Meneghini, J.F. Viens, A. Villeneuve. Non-linear optical properties of chalcogenide glasses in the system As–S–Se. J. Non-Cryst. Solids. 1999, Vols. 256-257, 353-360.
32. T. Kohoutek, T. Wagner, J. Orava, M. Krbal, A. Fejfar, T. Mates, S.O. Kasap, M. Frumar. Surface morphology of spin-coated As–S–Se chalcogenide thin films. J. Non-Cryst. Solids. 2007, Vol. 353, 13, 1437-1440.
33. W.W. Mullins. Flattening of a Nearly Plane Solid Surface due to Capillarity. J. Appl. Phys. 1959, Vol. 30, 1, 77-83.
34. K. Palka, J. Jancalek, S. Slang, M. Grinco, M. Vlcek. Comparison of optical and chemical properties of thermally evaporated and spin-coated chalcogenide AsS thin films targeting electron beam lithography applications. J. Non-Cryst. Solids. 2019, Vol. 508, 7-14.
35. S.N. Yannopoulos. Structure and photo-induced effects in elemental chalcogens: a review on Raman scattering. J. Mater. Sci. Mater. 2020, Vol. 31, 7565–7595.
36. B. Yang, D.J. Xue, M. Leng., J. Zhong, L. Wang, H. Song, Y. Zhou, J. Tang. Hydrazine solution processed Sb2S3, Sb2Se3 and Sb2(S1−xSex)3 film: molecular precursor identification, film fabrication and band gap tuning. Sci. Rep., Vol. 5, 1, 10978.
37. C.G. Pantano, T.A. Guiton. Sol-to-gel and gel-to-glass transitions in the As2S3-amine system. Chem. Mater. 1989, Vol. 1, 5, 558-563.
38. Ch. Wang, H. Chen, W. Dong, J. Ge, W. Lu, X. Wu, L. Guo, L. Chen. Sulfur–amine chemistry-based synthesis of multiwalled carbon nanotube–sulfur composites for. Chem.Commun. 2014, Vol. 50, 10, 1202-1204.

39. F.-Y. Lin, O. Gulbiten, Z. Yang, L. Calvez, P. Lucas. Mechanism of photostructural changes in mixed-chalcogen As–S–Se glasses investigated by Raman spectroscopy. J. Phys. D: Appl. Phys. 2011, Vol. 44, 4, 045404.
40. A. Stronski, L. Revutska, A. Meshalkin, O. Paiuk, E. Achimova, A. Korchovyi, K. Shportko, O. Gudymenko, A. Prisacar, A. Gubanova, G. Triduh. Structural properties of Ag–As–S chalcogenide glasses in phase separation region and their application in holographic grating recording. Opt. Mater. 2019, Vol. 94, 393-397.
41. Prince, R. Singh, M. Zulfequar, A. Kumar, P.K. Dwivedi. Electrical and optical properties of solution phase deposited As2S3 and As2Se3 chalcogenide thin films: A comparative study with thermally deposited films. J. Non-Cryst. Solids. 2017, Vol. 476, 46-51.